Special Collection

Dynamic Impedance Spectroscopy of Nickel Hexacyanoferrate Thin Films

Collins Erinmwingbovo, Dominique Koster, Doriano Brogioli, and Fabio La Mantia*[a]

Dynamic multi-frequency analysis (DMFA) is capable of acquiring high-quality frequency response of electrochemical systems under non-stationary conditions in a broad range of frequencies. In this work, we used DMFA to study the kinetics of (de-)intercalation of univalent cations (Na^+ and K^+) in thin films of nickel hexacyanoferrate (NiHCF) during cyclic voltammetry. For this system, the classic stationary electrochemical impedance spectroscopy fails due to the instability of the oxidized form of NiHCF. We are showing that such spectra can be fitted with a physical model described by a simple two-step intercalation mechanism: an adsorption step followed by an insertion step. The extracted kinetic parameters are depending on the state of charge as well on the nature of the inserted cation.

1. Introduction

Dynamic multi-frequency analysis (DMFA) has been proposed as a new method for the acquisition of high quality dynamic impedance spectra and extraction of kinetic parameters of electrochemical systems under non-stationary conditions i.e. while their properties are changing due to an on-going process.[1–3] This method is based on a multi-sine excitation, which perturbs a time variant system. By using quadrature filters, it is possible to simultaneously evaluate the dynamic impedance in a broad range of frequencies as a function of the time domain. In contrast to that, in classic electrochemical impedance spectroscopy (EIS), different frequencies perturb the system successively,[4–6] rendering this tool unsuited for time evolving electrochemical systems.

The concept of dynamic impedance spectroscopy has evolved over the years since its inception in the 1970s by Bond et al.,[7,8] who superimposed a multi-sine potential onto a DC triangular waveform with a ramp or staircase potential variation and thus allowing measuring the admittance as a function of the DC potential. This technique was further developed in the late 1990s by Haze et al.[9] The advances in information technology allowed for the development of microcomputer-based instrumentation, which enabled high quality Fourier transform to be used to extract impedance spectra over a wide range of frequencies and DC potentials. Since the system is time variant, the accuracy of the Fourier transform is rather low,

due to the presence of spectral leakage.[3] The interferences increase with the degree of non-stationarity and non-linearity of the system, as well as with a decrease in frequency of the multi-sine.[2,10] Hence, Stoynov et al. reported a numerical method that allows for the estimation of the errors that occur due to the time delay during measurement.[11]

Recently, the concept of DMFA and analysis of non-stationary impedance using classic electrical equivalent circuit (EECs) was reported by our research group.[1] Subsequently, it was shown that it is possible to obtain high quality impedance spectra by optimizing the parameters in the multi-sine such as frequency distribution and distance between successive frequencies as well as by a proper choice of a quadrature filter.[2] This means that, instead of analyzing the data in pieces in the time domain, a large amount of data (millions of points) are transformed in the frequency domain, where they are then separated in different frequency intervals and properly filtered.[3] This technique was tested on redox couples[1,2] and then successfully used for extracting kinetic parameters during hydrogen evolution[12] and silicon electro-dissolution.[13]

In this work, we applied DMFA in studying the reaction kinetics of nickel hexacyanoferrate (NiHCF) thin film. The interest in thin films of Prussian blue derivatives is connected to their fast charging/discharging rates,[14,15] large ion-exchange capacities,[16] low cost and low toxicity,[17] which makes them interesting materials in various applications such as electrochemically switched ion exchange (ESIX),[18,19] ion sensing,[20,21] electrocatalytic,[22,23] electrochromic and photo-magnetic applications.[24–28] The chemical formula of NiHCF is $A_nNiFe(CN)_6$, in which A is the intercalated cation.[16,29] NiHCF has been described as a non-selective host structure and the reversible insertion of various cations (Li^+, Na^+, K^+, Cs^+, NH_4^+) in this material from single and mixed solutions has been reported.[30–38]

The (de-)intercalation of cations in NiHCF has been attributed to the (reduction) oxidation of the iron centers followed by the (de-)insertion of cations in the NiHCF in order to preserve the electroneutrality of the host structure.[31,38] NiHCF shares the open framework structure and electrochem-

[a] C. Erinmwingbovo, D. Koster, Dr. D. Brogioli, Prof. F. La Mantia
Universität Bremen, Energiespeicher- und Energiewandlersysteme, Bibliothekstr. 1, 28359 Bremen, Germany
E-mail: lamantia@uni-bremen.de

ical behavior of other cyanometallates.[39–42] The large interstitial sites within this open framework allows reversible insertion of various cations or zeolitic water.[41–43] Thin films of NiHCF have been successfully grown by two methods: anodic derivatization from a nickel surface[44] and cathodic deposition onto a conductive substrate.[31] In anodic derivatization, the film forms upon oxidation of metallic nickel to divalent nickel ions, which precipitate as NiHCF on the electrode's surface in the presence of ferricyanide anions. In cathodic deposition, a metastable solution containing ferricyanide and divalent nickel is used; reduction of the ferricyanide on an inert surface leads to precipitation of NiHCF analogously to Prussian blue deposition. Ion-exchange capacities for cathodically deposited films are normally much greater than those for anodically derivatized films, though many of their cation intercalation traits appear identical.[16,45]

It has been reported that cathodically deposited NiHCF thin films are more similar to the "insoluble" Prussian Blue i.e. $A_4Ni_4^{II}[Fe^{II}(CN)_6]_3$, than the "soluble" form $(A_2Ni^{II}[Fe^{II}(CN)_6]_4)$.[16] It is interesting to stress that cathodically deposited NiHCF has been reported to be unstable[46] and it tends to undergo irreversible changes during cycling, thus making this system difficult to study by means of conventional stationary electrochemical impedance spectroscopy. Such systems may experience degradation during the acquisition of the low frequencies impedance data and could lead to impedance spectra showing uncommon shapes such as inductive loops which leads to incorrect interpretation of reaction mechanisms. This could be one of the reason for the peculiar shape of the impedance spectra reported by Ventosa et al. who have shown for similar films impedance spectra with inductive loop in the low frequency region.[47] Other possible reason for the inductive loops in the low frequency region could be artefacts from the cell set-up and the reference electrode. It has been reported that if the impedance of the reference electrode is around 10 kΩ, its coupling with the inherent stray capacitance of the potentiostat may generate distortions in the range of kHz.[48,49] The classic impedance spectra are acquired in the direction of decreasing frequencies with a certain logarithmically spaced data point density. At high frequencies, the data can be acquired in a short time and hence the drift would have very little effect, however at low frequencies, drift effects would be relatively large and could become significant.[50] Herein we show that DMFA has the advantage of the simultaneous acquisition of all frequencies at each potential and the ability to acquire impedance spectra while cycling, which make it suitable for the study of kinetics of unstable electrochemical systems and understanding the mechanisms of reactions occurring in such systems.

2. Results and Discussions

2.1. Film Growth

NiHCF thin film growth was observed on the electrode surface while cycling the potential from 0.85 V to 0.00 V vs Ag/AgCl in the electrodeposition solution described in the experimental
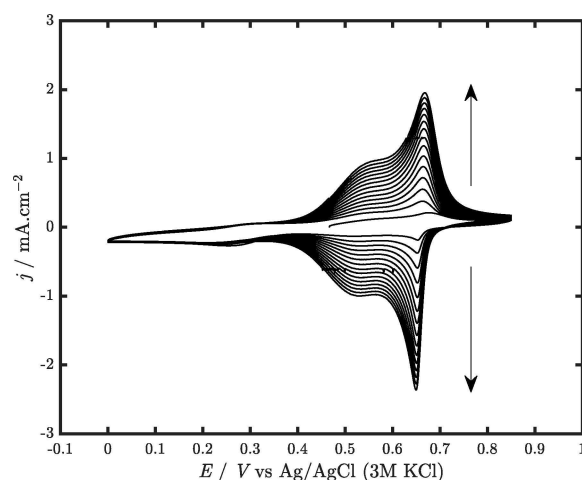
Figure 1. Cyclic voltammogram obtained during the electrodeposition of NiHCF in a freshly prepared solution of 2 mM $K_3Fe(CN)_6$, 2 mM $NiSO_4$ and 0.5 M K_2SO_4 using a scan rate of 25 mVs^{-1}.

section. Increase in the anodic and cathodic peak current of the voltammogram, as well as the circulating charge were observed as the cycle number increased as shown in Figure 1. The peaks are associated to the (de-)intercalation of K^+ in the NiHCF; the increase of the peaks follows the growth of the film thickness. The film growth has been reported to proceed during the reductive potential scans when $[Fe(CN)_6]^{3-}$ is reduced to $[Fe(CN)_6]^{4-}$ and instantaneously reacts with Ni^{2+} and K^+ present in solution to form sparingly soluble nickel(II) hexacyanoferrate(II) deposit on the electrode surface with the formula $K_2Ni[Fe(CN)_6]$.[31]

The voltammogram obtained during the electrodeposition exhibited a shouldered peak (Figure 1) which has been attributed to the reversible insertion of K^+ in two stable forms of the NiHCF.[31] The shouldered peak could also be attributed to interactions between redox sites and intercalated sites. An ideal curve with well-defined shape is obtained for the ideal model where NiHCF is assumed to be an ideal solution. This is often not the case as we have reported in our previous publication.[29] The deposition of the film is stopped when the voltammogram becomes stable upon cycling as seen in Figure 1. The charge consumed on reduction of the electrodeposited NiHCF thin film was calculated from the integral of the cathodic part of the cyclic voltammogram and it was equal to . 5.9 mC·cm^{-2}. The thickness of the film estimated from the charge was ca. 100 nm.

2.2. Structural Characterization of Film

The surface morphology of the electrodeposited NiHCF suggests that the film deposited on the GCE surface is not compact. Particle agglomeration was observed in the SEM image obtained (Figure 2a). The elements K, Ni, Fe, C and N were detected in the EDXA spectra (Figure 2b). The high carbon content originates from the GCE electrode. The Fe:K:Ni ratio was estimated to be 1:1:1.4 from the EDS results suggesting a
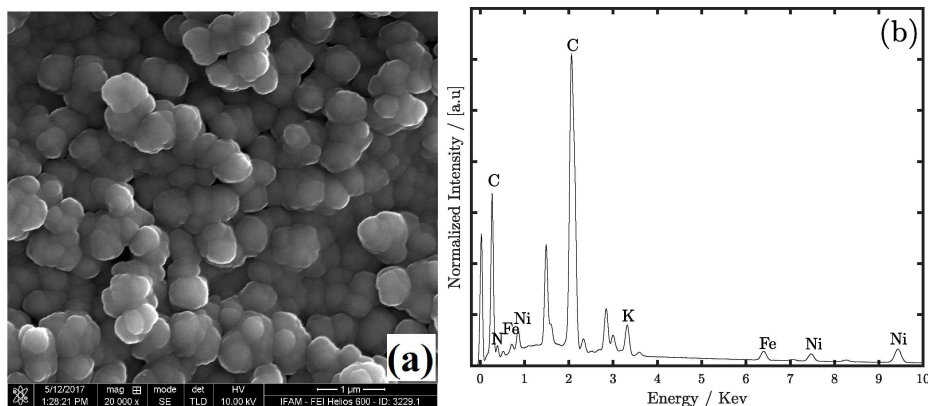
Figure 2. (a) SEM image of the GCE electrode surface covered with NiHCF (b) EDX pattern of the GCE electrode surface covered with NiHCF.

chemical formula $KNi_{1.42}[Fe(CN)_6]$, similar to what has been reported in literature as the insoluble form of the Prussian blue derivative.[16,51]

2.3. Quasi Cyclic Voltammogram

The deposited NiHCF was tested in solutions containing K^+ and Na^+ ions by applying the quasi-triangular wave at a scan rate of $200\ mV\,s^{-1}$. The voltammogram (Figure 3) shows peaks associ-
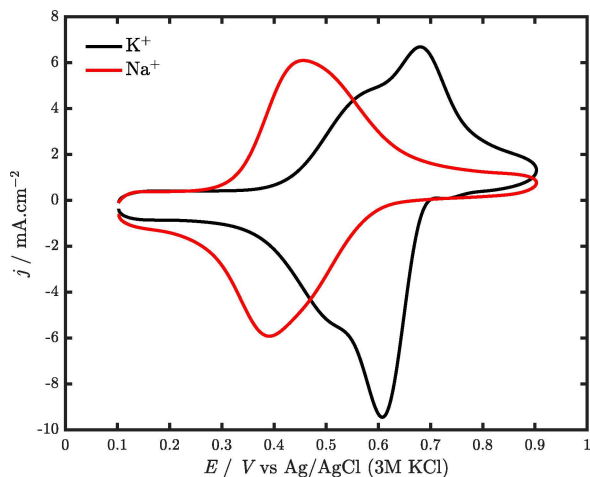

Figure 3. Cyclic voltammogram obtained from the quasi triangular wave applied to the NiHCF thin films in 0.5 M A_2SO_4 solution (A = K, Na) using a scan rate of $200\ mV\,s^{-1}$.

ated with the reversible insertion of both cations (K^+ and Na^+) with K^+ exhibiting a shouldered peak. In contrast to the shouldered peak observed in K^+, the voltammogram obtained during the (de-)insertion of Na^+ exhibited a single peak. The reversible insertion of univalent cations in NiHCF is depicted below in Equation (1):

$$ANi[Fe^{III}CN_6] + A^+ + e^- \rightleftharpoons A_2Ni[Fe^{II}CN_6] \tag{1}$$

The peak potential for the reversible insertion of the cations follows the hydrated radii as reported widely in literature.[29,52,53] The difference between the cathodic and the anodic peak (ΔE_p) for Na^+ and K^+ was ca. 60 mV and 80 mV respectively. This low ΔE_p at a scan rate of $200\ mV\,s^{-1}$ indicates that the charge transfer kinetics is fast.

Hao et al. reported that NiHCF thin films deposited using the cathodic deposition method are quite unstable and exhibit ca. 60% charge retention after 500 cycles while cycling at $10\ mV\,s^{-1}$.[46] To this end, the stability of the oxidized and reduced form was studied to ascertain what potential the NiHCF film can be held before polarization with the multi-sine wave. The result obtained (Figure S1b in the supporting information) indicates that the reduced form of NiHCF is more stable than the oxidized form.

2.4. Dynamic Multifrequency Analysis and Equivalent Circuit Proposed for Fitting Impedance Spectra

The dynamic impedance Z′ can be defined as Equation (2);

$$Z' = \frac{iFT[\Delta U(\omega).g(\omega'-\omega),bw]}{iFT[\Delta I(\omega).g(\omega'-\omega),bw]} \tag{2}$$

where ΔU and ΔI are the Fourier transform of the potential and the current signals respectively, ω is the angular frequency, g is a quadrature filter function, and bw is the bandwidth of the quadrature filter. In this work, we used a quadrature filter function as reported in Equation 3, where n is equal to 8, and the bandwidth used was 5 Hz. The purpose of the procedure is to optimally resolve the impedance as a function of time and frequencies. The shape of g is similar to a flat-top filter.

$$g(\omega'-\omega,bw) = \frac{[1+\exp(-n)]^2}{\left[1+\exp\left(-n\frac{\omega'-\omega+bw}{bw}\right)\right]\left[1+\exp\left(-n\frac{\omega'-\omega-bw}{bw}\right)\right]} \tag{3}$$
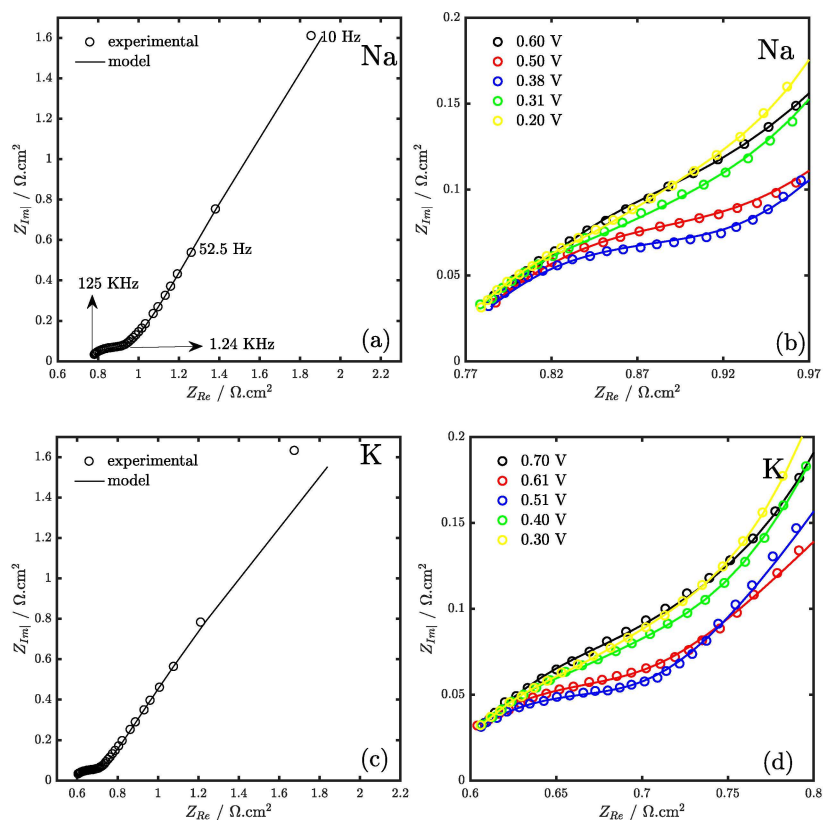
Figure 4. Nyquist plot of impedance spectra obtained in the cathodic scan of NiHCF thin film within the frequency range of 10 Hz to 125 kHz in (a) 0.5 M Na$_2$SO$_4$ solution at 0.38 V (b) High-frequency region of the impedance spectra obtained at different potentials during the cathodic scan in 0.5 M Na$_2$SO$_4$ (c) 0.5 M K$_2$SO$_4$ solution at 0.51 V (d) High-frequency region of the impedance spectra obtained at different potentials during the cathodic scan in 0.5 M K$_2$SO$_4$.
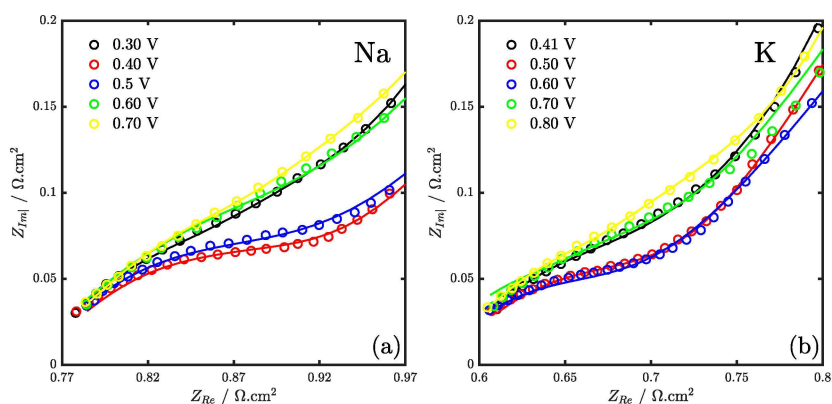

Figure 5. Nyquist plot of the high-frequency region of the impedance spectra obtained at different potentials during the anodic scan in 0.5 M (a) Na$_2$SO$_4$ and (b) K$_2$SO$_4$.

The impedance spectra obtained in 0.5 M Na$_2$SO$_4$ and K$_2$SO$_4$ at different potential during the cathodic and anodic scan are shown in Figure 4 and Figure 5. The impedance spectra comprises of a potential dependent depressed semicircle occurring in the high frequency region terminated by a straight line occurring at an angle less than 90° in the low frequency region which has been attributed to a solid-state diffusion in a porous electrode system.[54]

The measured impedance spectra were fitted using a model, which assumes that the reversible insertion of the cations occurs through a two-step process: the first step is the ion-sorption followed by an the reversible insertion of the cation with a subsequent change in the oxidation state of Fe from +3 to +2 to achieve charge neutrality (second step) [Eqs. (4) and (5)]:

$$A_\varepsilon^+ \rightleftharpoons A_i^+ \tag{4}$$

$$A_i^+ + ANi[Fe^{III}CN_6] + e^- \rightleftharpoons A_2Ni[Fe^{II}CN_6] \tag{5}$$
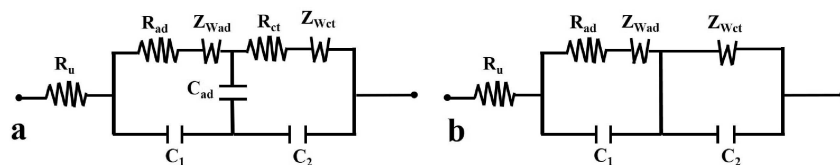
Figure 6. (a) Equivalent circuit obtained from the modelling the reversible insertion of cations in aqueous electrolyte as a two-step process (b) Equivalent circuit used for fitting the measured impedance data obtained from statistical analysis of the equivalent circuit from the model.

where the subscript ε and i indicate the solution and the inner Helmholtz plane (IHP).

Detailed mathematical description of this model can be found in the supporting information. The equivalent circuit obtained from the model (Figure 6a) consists of the uncompensated cell resistance (R_u), resistance of adsorption (R_{ad}), Warburg impedance in the electrolyte (Z_{Wad}), which is defined as $Z_{Wad} = \sigma_{ad} \cdot (j\omega)^{-0.5}$, adsorption capacitance (C_{ad}), charge transfer resistance (R_{ct}), Warburg impedance in the solid (Z_{Wct}) described using the finite length diffusion with a reflective boundary $Z_{Wct} = (\sigma_{ct}(j\omega)^{-0.5}) \cdot \coth\sqrt{j\omega\tau}$.[55] C_1 and C_2 denotes the capacitance of the outer and inner Helmholtz plane respectively.

To avoid over parametrization of the equivalent circuit by physicochemical processes that are very fast or very slow with respect to the the frequency range used in this work, the parameters obtained from the fit were subjected to t-test as shown in a recent publication:[12] Equation (6):

$$ t = \frac{\hat{x}}{\sigma_{\bar{x}}} \tag{6} $$

where $\hat{x}$ is the estimated parameters from the fit of the measured impedance and the model and $\sigma_{\bar{x}}$ is the absolute standard error of the parameters which is obtained from the formal covariance matrix of χ^2 minimization.[12] Starting from the equivalent circuit in Figure 6a, we removed the parameters which were failing the t-test until all parameters were above the significance interval of 95%. The resulting equivalent circuit shown in Figure 6b which is obtained from the model with the assumption that the C_{ad} is much higher than the inner Helmholtz plane capacitance. The equivalent circuit also takes into account that R_{ct} is very small (i.e. fast insertion process). In our model, R_{ct} takes into account the limitations due to the further desolvation of the partial desolvated cations and transfer of the desolvated cations across the electrode/electrolyte interface. The hydrated radii of Na$^+$ and K$^+$ has been reported as 1.83 Å and 1.25 Å respectively while the channels connecting the intercalation sites has been reported to be 1.6 Å,[22,39] thus it is plausible that the cations are intercalated in their partially desolvated state resulting in the charge transfer process becoming extremely fast. The solid-state transport in the solid in the equivalent circuit (Figure 6b) was also described using the simpler semi-infinite diffusion against the classic finite length diffusion with reflective boundary used for intercalation electrode. This assumption is valid when $\tilde{\omega} \gg 1$ where $\tilde{\omega}$ is the diffusion characteristic frequency,[56] i.e. when the diffusion time

is generally long with respect to the investigated frequency. Further details of the statistical analysis and process for selecting the equivalent circuit can be found in the supporting information.

For fitting the data, the transmission line model (TLM) used to describe Faradaic processes occurring in porous electrode system[57–60] was used in this work. This choice is supported not only from the quality of the fitting and shape of the impedance spectra but also from the SEM images which suggest that the electro-deposited NiHCF is not compact. Schematics of the TLM model is shown in Figure S2 in the supporting information. In this study, we use the simplified TLM model for cylindrical pores in describing the Faradaic process.[59] The mathematical description of the simplified TLM model is given by Equation (7):[59]

$$ Z_T(\omega) = R_u + R_p \left[\frac{\coth(kl)}{kl} \right] \tag{7} $$

where Z_T is the total impedance of the electrode, R_p is the resistance of the pores, l is the thickness of the pore and κ is a dimensionless parameter.The impedance of single reacting sites which is represented by the term κl.[59] For fitting the impedance spectra, an algorithm based on the non-linear least squares minimization with an additional constraint on the smoothing of the fitting parameter was used, as reported in.[1] More details of the fitting algorithm can be found in section S4 of the supporting information. The model fitting procedure of the experimental impedance data had a standard deviation, χ^2 in the range of $1.3 \cdot 10^{-5}$ to $6.0 \cdot 10^{-5}$.

In addition to this, we want to stress that the spectra obtained in this work were in contrast with what has been reported by Ventosa et al. for NiHCF and Prussian blue thin films,[47] where the impedance spectra obtained in NiHCF thin film in aqueous and non-aqueous solutions of univalent cations in the frequency range of 50 kHz to 100 mHz exhibited an inductive loop in low frequency region. As discussed in the introduction, the origin of this loop could be caused by the instability of the thin films or by artefacts arising from the electrochemical setup. We did not observe the inductive loop in any of the performed experiments, even in static conditions. The results obtained in this work confirms the advantages of DMFA coupled with an optimised set-up over conventional static EIS in studying the kinetics of unstable or evolving electrochemical systems.

2.5. Dependence of the Kinetic Parameters on the Variation of Electrode Potential

The R_{ad} obtained from the fit for both cations is shown in Figure 7 and exhibited a dependence on the electrode potential
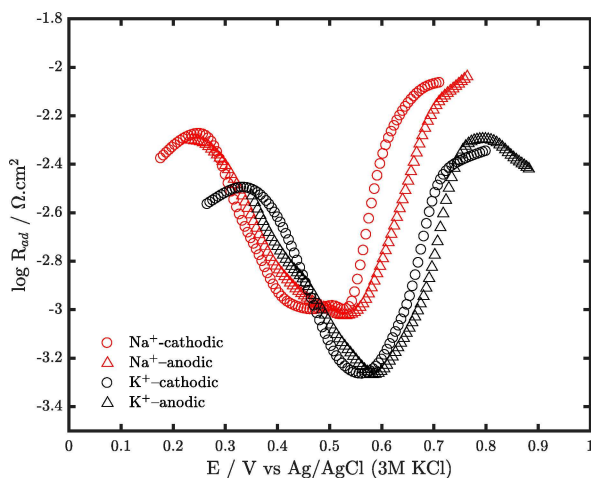
Figure 7. Variation of the resistance of adsorption (R_{ad}) on the electrode potential.

with a minimum around the peak potential in the cyclic voltammogram.

The potential dependence of R_{ad} is explained by the description of R_{ad} obtained from the model which is given by Equation (8):

$$R_{ad} = \frac{RT}{F^2 k_1^0 \left[\frac{C_{A_r}}{C_0}\right]^{1-\alpha_1} [1-\beta]^{1-\alpha_1} \beta^{\alpha_1}} \quad (8)$$

where F is Faraday's constant, T is absolute temperature in Kelvin, k_1^0 is the standard rate constant of the desolvation step, β represents the molar fraction of the adsorbed species and α_1 represents the transfer coefficient for the desolvation step. Equation 8 predicts a decrease in the R_{ad} when $\beta \leq 0.5$ and increases when $\beta \geq 0.5$ with a minimum when $\beta = 0.5$ which occurs close to the peak potential in the voltammogram assuming a fractional coverage for β. The assumption of a fractional coverage for β is explained in section S7 of the supporting information. The experimental result was observed to be in good agreement with the model prediction with a single minimum observed for both cations. The R_{ad} for the de-insertion of Na$^+$ and K$^+$ obtained from the fit was in the same order of magnitude which can be attributed to similarity in the hydrated radii of the cations (Na$^+$ = 1.83 Å; K$^+$ = 1.25 Å).[39,61]

Figure 8 shows the dependence of σ_{ad} which describes the mass transport resistance of the desolvated cation in the OHP on electrode potential. σ_{ad} showed a dependency on the electrode potential and a minimum is observed for both cations in the potential region close to the cathodic/anodic peak in the cyclic voltammogram, as observed also in the electron transfer
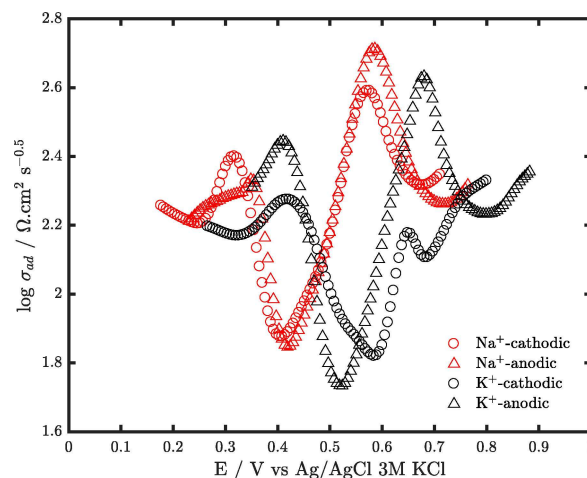
Figure 8. Dependence of the Warburg coefficient in the electrolyte (σ_{ad}) on the electrode potential.

reaction from/to a redox couple.[1] A comparison of the minimum σ_{ad} for Na$^+$ and K$^+$ indicates that the mass transport limitations are similar for both cations which can be attributed to a similar diffusion coefficient of both cations in aqueous solutions (Na$^+$ = $1.33 \cdot 10^{-5}$ $cm^2 s^{-1}$ and K$^+$ = $1.96 \cdot 10^{-5}$ $cm^2 s^{-1}$).[62]

The σ_{ct} reported in Figure 9 represents the resistance of the mass transport of the cations in the NiHCF lattice. The σ_{ct} curve
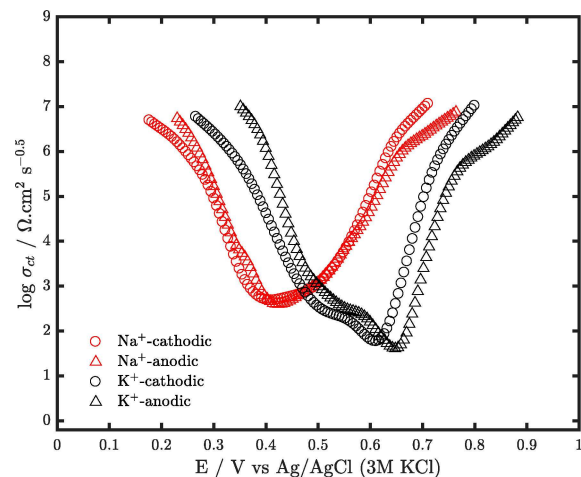
Figure 9. Variation of the Warburg coefficient in the solid (σ_{ct}) on the electrode potential.

was similar to the current potential curve which can be attributed to the fact that Warburg impedance in the solid can be described $Z_{Wct} = \sigma_{ct}\omega^{-0.5}/\sqrt{2} - j\sigma_{ct}\omega^{-0.5}/\sqrt{2}$, where the second term corresponds to a pseudo-capacitance (C_W).[55,56] This explains the shape of the plot of σ_{ct} vs the electrode potential as the product of C_W and the scan rate is the charge of the reversible insertion process. The mass transport resistance was observed to be similar for both cations probably due to the similar ionic radius of the cations. The diffusion of different

cations in the same intercalating electrode depends on the size of the inserted cation.[63]

The result obtained from this study suggests that the kinetics of the reversible insertion of cations in NiHCF thin films depends on the electrode composition as well as the inserted cation. It is observed that the kinetic parameters obtained for the cations studied (Na^+ and K^+) are in the same order of magnitude indicating similar rates in the kinetics of the de-insertion of the cations. The similarity in kinetic parameters is related to the ionic and hydrated radii of the cations which plays an important role in the kinetics of de-insertion process of cations in aqueous medium.

3. Conclusion

The results obtained from this study shows that DMFA as a technique coupled with an optimised electrochemical cell set-up can be used for studying the kinetics of unstable electrochemical system which are difficult to study using the classic electrochemical impedance spectroscopy due to drift effects. DMFA allows for the elucidation of reaction mechanism and extraction of kinetic parameters of such unstable electrochemical systems. The kinetics of the de-insertion of univalent cations (Na^+ and K^+) in NiHCF thin film made by cathodic deposition which exhibits instability in its oxidized form was studied using DMFA. High-quality impedance spectra were obtained and fitted using the transmission line model (TLM) for porous electrode in an equivalent circuit obtained from modelling the reversible insertion of cation in NiHCF as a two-step process. The first step corresponds to the partial desolvation of the cation and it is followed by an insertion step, during which change in the oxidation state in the cathode material occurs. This is at variance with some literature, in which by using static impedance a three step mechanism was proposed.[47] We attributed the observed differences between literature and our results to instability of the thin film and/or distortions due to the cell geometry or reference electrode. The kinetic parameters for both cations (Na^+ and K^+) were observed to be in the same order of magnitude indicating similar rates of the kinetic processes which was attributed to similarity in ionic and hydrated radii of the inserted cations. The result obtained in this work highlights the possible application of DMFA in studying the kinetics of cathode and anode materials for batteries, super capacitors and ion pumping techniques allowing for a deeper understanding of the underlying mechanism in these materials which is needed for the optimization of these technologies.

Experimental Section

The chemicals used in this study were analytical grade materials and were used as received without further modification. Solutions were prepared using deionized water and all electrochemical measurements were carried out at room temperature. The electrochemical experiments were performed in a three-electrode cell consisting of a 1 mm diameter glassy carbon electrode (GCE) as the

working electrode (WE), a platinum mesh (Labor Platina) as the counter electrode (CE) and Ag/AgCl (3 M KCl) as the reference electrode (RE). The relative potential of the Ag/AgCl (3 M KCl) to the potential of the standard hydrogen electrode was $+0.197$ V. Artefacts related to the reference electrode where minimized by using a 100 nF capacitive bridge between the CE and RE as reported in reference,[48] with a similar cell setup. This cell geometry has significant advantages such as reproducibility, minimization of the current line distribution, insensitivity to the position of the RE.[64] Electrochemical measurements were done using Bio-Logic SP300 Potentiostat which was connected to a two channel oscilloscope 4262 PicoScope (Pico technology) as well as to a two channel 33512b waveform generator (Keysight) where home-made MATLAB scripts (release 2015b from the Math Works Inc.) were used to create the desired potential profile of the multi-sine signal as described in reference.[2]

Electrodeposition of NiHCF

NiHCF thin films were electrodeposited using the cathodic deposition technique.[31] Briefly, 1 mm diameter GCE was cycled from 0.85 V to 0.00 V vs Ag/AgCl 3 M KCl using a scan rate of 25 mV s^{-1} in a freshly prepared solution of 2 mM $K_3FeCN)_6$ (Sigma-Aldrich), 2 mM $NiSO_4$ (Sigma-Aldrich) and 0.5 M K_2SO_4 (Sigma-Aldrich). Before cycling, the GCE electrode was polished using 0.250 μm, and 0.1 μm polishing pads (Struers) with the corresponding diamond suspension (Struers) on a polishing machine with 300 rpm. After polishing, the electrode was sonicated in water for 3 minutes and then cleaned electrochemically by cycling in 1 M H_2SO_4 from 1.5 V to -0.250 V vs Ag/AgCl using a scan rate of 25 mV s^{-1}.

Scanning Electron Microscopy (SEM) and Energy-Dispersive X-ray spectroscopy (EDXA)

Surface morphology of the NiHCF-covered GCE electrode were studied using scanning electron microscopy (SEM, FEI Helios NanoLabTM 600 DualBeamTM). Elemental composition of the electrodeposited NiHCF thin films were studied using EDXA. The accelerating voltage used to stimulate the X-ray emission was 15 keV. X-rays with energies between 0 and 10 keV were collected and used in identification of the elements using AZTEC 3.3 software from Oxford instruments.

Electrochemical Characterization

The 1 mm diameter GCE covered with NiHCF was tested in solutions containing K^+ and Na^+ at concentration of 0.5 M. The electrode was polarized at 100 mV vs Ag/AgCl, to which the quasi-triangular wave (Figure S1a in the supporting information). and the multi-sine generated by the arbitrary waveform generator were added. The quasi-triangular wave was already described in previous publication of our research group.[2] The current range used for all experiments was 1 mA. The frequency of the quasi-triangular wave was chosen to be 0.125 Hz, corresponding to a scan rate of 200 mV s^{-1}. The base frequency for the multi-sine was 1.25 Hz, thus the impedance data covered the frequency range from 10 Hz to 125 kHz. The amplitude of the quasi-triangular and multi-sine was 400 mV and 175 mV peak to peak respectively. The waveform was smoothed using the incorporated Trueform^{TM} filter function in the frequency generator. 10 million samples were recorded in each measurement with a sample rate of 1 μs. 200 impedance spectra were fitted for each cation (100 each for cathodic and anodic polarization); 20 spectra per cation are shown in the supporting information. Details of the design of the frequency distribution of the multi-sine used in this work is described in detail elsewhere.[2]

The data evaluation was performed using suitable home-made MATLAB scripts.

Acknowledgement

Conflict of Interest

The authors declare no conflict of interest.

[1] A. Battistel, G. Du, F. La Mantia, *Electroanalysis* **2016**, *28*, 2346–2353. doi:10.1002/elan.201600260.

[2] D. Koster, G. Du, A. Battistel, F. La Mantia, *Electrochim. Acta* **2017**, *246*, 553–563. doi:10.1016/j.electacta.2017.06.060.

[3] A. Battistel, F. La Mantia, *Electrochim. Acta* **2019**, *304*, 513–520. doi:10.1016/J.ELECTACTA.2019.03.033. URL https://www.sciencedirect.com/science/article/pii/S001346861930427X

[4] M. E. Orazem, B. Tribollet, Electrochemical impedance spectroscopy, second edition Edition, The ECS series of texts and monographs, Wiley Blackwell, Hoboken, NJ, 2017.

[5] D. J. Zahniser, J. F. Brenner, *Cytometry* **1985**, *6*, 392. doi:10.1002/cyto.990060420.

[6] H. Cesiulis, N. Tsyntsaru, A. Ramanavicius, G. Ragoisha, The study of thin films by electrochemical impedance spectroscopy, in: I. Tiginyanu, P. Topala, V. Ursaki (Eds.), Nanostructures and thin films for multifunctional applications, NanoScience and Technology, Springer Berlin Heidelberg, New York NY, 2016, pp. 3–42. doi:10.1007/978-3-319-30198-3 1.

[7] A. M. Bond, R. J. Schwall, D. E. Smith, *J. Electroanal. Chem. Interfacial Electrochem.* **1977**, *85*, 231–247. doi:10.1016/S0022-0728(77)80290-8.

[8] R. J. Schwall, A. M. Bond, D. E. Smith, *J. Electroanal. Chem. Interfacial Electrochem.* **1977**, *85*, 217–229. doi:10.1016/S0022-0728(77)80289-1.

[9] J. Házì, D. M. Elton, W. A. Czerwinski, J. Schiewe, V. A. Vicente-Beckett, A. M. Bond, *J. Electroanal. Chem.* **1997**, *437*, 1–15. doi:10.1016/S0022-0728(96)05038-3.

[10] Z. B. Stoynov, B. S. Savova-Stoynov, *J. Electroanal. Chem. Interfacial Electrochem.* **1985**, *183*, 133–144. doi:10.1016/0368-1874(85)85486-1.

[11] Z. Stoynov, *Electrochim. Acta* **1993**, *38*, 1919–1922. doi:10.1016/0013-4686(93)80315-Q.

[12] D. Koster, A. R. Zeradjanin, A. Battistel, F. La Mantia, Extracting the kinetic parameters of the hydrogen evolution reaction at Pt in acidic media by means of dynamic multi-frequency analysis, Electrochimica Acta (apr 2019). doi:10.1016/J.ELECTACTA.2019.04.013. URL https://www.sciencedirect.com/science/article/pii/S0013468619306887

[13] D. Koster, M. Patzauer, M. M. Salman, A. Battistel, K. Krischer, F. La Mantia, *ChemElectroChem* **2018**, *5*, 1548–1551. doi:10.1002/celc.201800252. URL http://doi.wiley.com/10.1002/celc.201800252

[14] L. M. Siperko, T. Kuwana, *Electrochim. Acta* **1987**, *32*, 765–771. doi:10.1016/0013-4686(87)85107-1.

[15] C. Liu, Y. Wang, G. Zhu, S. Dong, *Electrochim. Acta* **1997**, *42*, 1795–1800. doi:10.1016/S0013-4686(96)00379-9.

[16] K. M. Jeerage, W. A. Steen, D. T. Schwartz, *Chem. Mater.* **2002**, *14*, 530–535. doi:10.1021/cm010156d.

[17] M. Omarova, A. Koishybay, N. Yesibolati, A. Mentbayeva, N. Umirov, K. Ismailov, D. Adair, M.-R. Babaa, I. Kurmanbayeva, Z. Bakenov, *Electrochim. Acta* **2015**, *184* 58–63. doi:10.1016/j.electacta.2015.10.031.

[18] X.-g. Hao, J.-x. Guo, S.-b. Liu, Y.-p. Sun, *Trans. Nonferrous Met. Soc. China* **2006**, *16*, 556–561. doi:10.1016/S1003-6326(06)60097-6.

[19] X. Hao, Y. Li, M. Pritzker, *Sep. Purif. Technol.* **2008**, *63*, 407–414. doi:10.1016/j.seppur.2008.06.001.

[20] L. J. Amos, A. Duggal, E. J. Mirsky, P. Ragonesi, A. B. Bocarsly, P. A. Fitzgerald-Bocarsly, *Anal. Chem.* **2002**, *60*, 245–249. doi:10.1021/ac00154a012.

[21] D. R. Coon, L. J. Amos, A. B. Bocarsly, P. A. Fitzgerald-Bocarsly, *Anal. Chem.* **1998**, *70*, 3137–3145. doi:10.1021/ac970975a.

[22] B. D. Humphrey, S. Sinha, A. B. Bocarsly, *J. Phys. Chem.* **1987**, *91*, 586–593. doi:10.1021/j100287a020.

[23] S. Sinha, B. D. Humphrey, A. B. Bocarsly, *Inorg. Chem.* **1984**, *23*, 203–212. doi:10.1021/ic00170a018.

[24] K. Itaya, K. Shibayama, H. Akahoshi, S. Toshima, *J. Appl. Phys.* **1982**, *53*, 804–805. doi:10.1063/1.329997.

[25] S. Demiri, M. Najdoski, J. Velevska, *Mater. Res. Bull.* **2011**, *46*, 2484–2488. doi:10.1016/j.materresbull.2011.08.021.

[26] D. M. DeLongchamp, P. T. Hammond, *Chem. Mater.* **2004**, *16*, 4799–4805. doi:10.1021/cm0496624.

[27] D. Aguilà, Y. Prado, E. S. Koumousi, C. Mathonière, R. Clérac, *Chem. Soc. Rev.* **2016**, *45*, 203–224. doi:10.1039/c5cs00321k.

[28] J. Agrisuelas, P. R. Bueno, F. F. Ferreira, C. Gabrielli, J. J. García-Jareño, D. Gimenez-Romero, H. Perrot, F. Vicente, *J. Electrochem. Soc.* **2009**, *156*, P74. doi:10.1149/1.3080711.

[29] C. Erinmwingbovo, M. S. Palagonia, D. Brogioli, F. La Mantia, *ChemPhysChem* **2017**, *18*, 917–925. doi:10.1002/cphc.201700020.

[30] L. F. Schneemeyer, S. E. Spengler, D. W. Murphy, *Inorg. Chem.* **1985**, *24*, 3044–3046. doi:10.1021/ic00213a034.

[31] J. Bácskai, K. Martinusz, E. Czirók, G. Inzelt, P. J. Kulesza, M. A. Malik, *J. Electroanal. Chem.* **1995**, *385*, 241–248. doi:10.1016/0022-0728(94)03788-5.

[32] J. Joseph, H. Gomathi, G. Prabhakara Rao, *Electrochim. Acta* **1991**, *36*, 1537–1541. doi:10.1016/0013- 4686(91)85003-P.

[33] M. A. Malik, K. Miecznikowski, P. J. Kulesza, *Electrochim. Acta* **2000**, *45*, 3777–3784. doi:10.1016/S0013-4686(00)00469-2.

[34] W. Chen, X. H. Xia, *Adv. Funct. Mater.* **2007**, *17*, 2943–2948. doi:10.1002/adfm.200700015.

[35] Q. Yu, W. A. Steen, K. M. Jeerage, S. Jiang, D. T. Schwartz, *J. Electrochem. Soc.* **2002**, *149*, E195. doi:10.1149/1.1474434.

[36] R. Trócoli, C. Erinmwingbovo, F. La Mantia, *ChemElectroChem* **2017**, *4*, 143–149. doi:10.1002/celc.201600509.

[37] X. Hao, D. T. Schwartz, *Chem. Mater.* **2005**, *17*, 5831–5836. doi:10.1021/cm0515101.

[38] W. Li, F. Zhang, X. Xiang, X. Zhang, *ChemElectroChem* **2017**, *4*, 2870–2876. doi:10.1002/celc.201700776. URL http://doi.wiley.com/10.1002/celc.201700776

[39] C. D. Wessells, R. A. Huggins, Y. Cui, *Nat. Commun.* **2011**, 2 550. doi:10.1038/ncomms1563.

[40] J. W. McCargar, V. D. Neff, *J. Phys. Chem.* **1988**, *92*, 3598–3604. doi:10.1021/j100323a055.

[41] W. Li, F. Zhang, X. Xiang, X. Zhang, *J. Phys. Chem. C* **2017**, *121*, 27805–27812. doi:10.1021/acs.jpcc.7b07920. URL http://pubs.acs.org/doi/10.1021/acs.jpcc.7b07920

[42] W. Li, F. Zhang, X. Xiang, X. Zhang, *ChemElectroChem* **2018**, *5*, 350–354. doi:10.1002/celc.201700958. URL http://doi.wiley.com/10.1002/celc.201700958

[43] M. Pasta, C. D. Wessells, R. A. Huggins, Y. Cui, *Nat. Commun.* **2012**, 3 1149. doi:10.1038/ncomms2139.

[44] A. B. Bocarsly, S. Sinha, *J. Electroanal. Chem. Interfacial Electrochem.* **1982**, *137*, 157–162. doi:10.1016/0022-0728(82)85075-4.

[45] S. D. Rassat, J. H. Sukamto, R. J. Orth, M. A. Lilga, R. T. Hallen, *Sep. Purif. Technol.* **1999**, *15*, 207–222. doi:10.1016/S1383-5866(98)00102-6.

[46] X. Hao, T. Yan, Z. Wang, S. Liu, Z. Liang, Y. Shen, M. Pritzker, *Thin Solid Films* **2012**, *520*, 2438–2448. doi:10.1016/j.tsf.2011.10.005.

[47] E. Ventosa, B. Paulitsch, P. Marzak, J. Yun, F. Schiegg, T. Quast, A. S. Bandarenka, The mechanism of the interfacial charge and mass transfer during intercalation of alkali metal cations, Advanced science (Weinheim, Baden-Wurttemberg, Germany) **2016**, *3*, 1600211. doi:10.1002/advs.201600211.

[48] A. Battistel, M. Fan, J. Stojadinović, F. La Mantia, *Electrochim. Acta* **2014**, *135*, 133–138. doi:10.1016/j.electacta.2014.05.011.

[49] F. Mansfeld, *J. Electrochem. Soc.* **1988**, *135*, 906. doi:10.1149/1.2095825.

[50] S. N. Victoria, S. Ramanathan, *Electrochim. Acta* **2011**, *56*, 2606–2615. doi:10.1016/j.electacta.2010.12.007.

[51] W. A. Steen, S.-W. Han, Q. Yu, R. A. Gordon, J. O. Cross, E. A. Stern, G. T. Seidler, K. M. Jeerage, D. T. Schwartz, *Langmuir* **2002**, *18*, 7714–7721. doi:10.1021/la020352e.

[52] C. D. Wessells, S. V. Peddada, M. T. McDowell, R. A. Huggins, Y. Cui, *J. Electrochem. Soc.* **2012**, *159*, A98. doi:10.1149/2.060202jes.

[53] H.-W. Lee, M. Pasta, R. Y. Wang, R. Ruffo, Y. Cui, *Faraday Discuss.* **2014**, *176*, 69–81. doi:10.1039/c4fd00147 h.

[54] Z. Gao, J. Bobacka, A. Ivaska, *Electrochim. Acta* **1993**, *38*, 379–385. doi:10.1016/0013-4686(93)85154-Q.

[55] A. Lasia, Electrochemical impedance spectroscopy and its applications, Springer, New York, 2014.

[56] J. Song, M. Z. Bazant, *J. Electrochem. Soc.* **2013**, *160*, A15–A24. doi:10.1149/2.023301jes. URL http://jes.ecsdl.org/lookup/doi/10.1149/2.023301jes

[57] R. de Levie, *Electrochim. Acta* **1963**, *8*, 751–780. doi:10.1016/0013-4686(63)80042-0.

[58] R. de Levie, *Electrochim. Acta* **1965**, *10*, 113–130. doi:10.1016/0013-4686(65)87012-8.

[59] F. La Mantia, J. Vetter, P. Novák, *Electrochim. Acta* **2008**, *53*, 4109–4121. doi:10.1016/j.electacta.2007.12.060.

[60] N. Ogihara, Y. Itou, T. Sasaki, Y. Takeuchi, *J. Phys. Chem. C* **2015**, *119*, 4612–4619. doi:10.1021/jp512564f.

[61] P. C. F. Pau, J. O. Berg, W. G. McMillan, *J. Phys. Chem.* **1990**, *94*, 2671–2679. doi:10.1021/j100369a080. URL http://pubs.acs.org/doi/abs/10.1021/j100369a080

[62] W. M. Haynes, CRC handbook of chemistry and physics, CRC Press, 2015. URL https://books.google.de/books/about/CRC Handbook of Chemistry and Physics 96.html?id =

[63] L. Chen, H. Shao, X. Zhou, G. Liu, J. Jiang, Z. Liu, *Nat. Commun.* **2016**, *7*, 11982. doi:10.1038/ncomms11982. URL http://www.nature.com/articles/ncomms11982

[64] J. Stojadinović, M. Fan, A. Battistel, F. La Mantia, *ChemElectroChem* **2015**, *2*, 1031–1035. doi:10.1002/celc.201500029.